Article

Current Biology

Double-Cone Localization and Seasonal Expression Pattern Suggest a Role in Magnetoreception for European Robin Cryptochrome 4

Highlights

- Double cones and long-wavelength single cones harbor cryptochrome 4 in birds
- Cry4 is upregulated during the migratory season in night-migratory European robins
- A homology model of the erCry4 structure predicts strong FAD binding
- Cry4 could be the primary magnetoreceptive protein in night-migratory songbirds

Authors

Anja Günther, Angelika Einwich, Emil Sjulstok, ..., Karl-Wilhelm Koch, Ilia A. Solov'yov, Henrik Mouritsen

Correspondence

henrik.mouritsen@uni-oldenburg.de

In Brief

Günther et al. suggest that Cry4 could be the magnetoreceptive protein in night-migratory songbirds. Cry4 seems to bind Flavin, shows only weak circadian oscillations, is specifically located in double cones and long-wavelength single cones, and is upregulated during the migratory season in night-migratory European robins but not in chicken.



Günther et al., 2018, Current Biology *28*, 211–223
January 22, 2018 © 2017 Elsevier Ltd.
https://doi.org/10.1016/j.cub.2017.12.003

CellPress

Current Biology
Article

CellPress

Double-Cone Localization and Seasonal Expression Pattern Suggest a Role in Magnetoreception for European Robin Cryptochrome 4

Anja Günther,[1,6] Angelika Einwich,[1,6] Emil Sjulstok,[2] Regina Feederle,[3] Petra Bolte,[1] Karl-Wilhelm Koch,[4,5] Ilia A. Solov'yov,[2] and Henrik Mouritsen[1,5,7,*]
[1]Institut für Biologie und Umweltwissenschaften, Carl-von-Ossietzky-Universität Oldenburg, Carl-von-Ossietzky-Strasse 9-11, 26129 Oldenburg, Germany
[2]Department of Physics, Chemistry and Pharmacy, University of Southern Denmark, Campusvej 55, 5230 Odense, Denmark
[3]Helmholtz Zentrum München, German Research Center for Environmental Health, Institute for Diabetes and Obesity, Monoclonal Antibody Core Facility, Ingolstädter Landstrasse 1, 85764 Neuherberg, Germany
[4]Department of Neuroscience, Carl-von-Ossietzky-Universität Oldenburg, Carl-von-Ossietzky-Strasse 9-11, 26129 Oldenburg, Germany
[5]Research Centre for Neurosensory Sciences, Carl-von-Ossietzky-Universität Oldenburg, Carl-von-Ossietzky-Strasse 9-11, 26129 Oldenburg, Germany
[6]These authors contributed equally
[7]Lead Contact
*Correspondence: henrik.mouritsen@uni-oldenburg.de
https://doi.org/10.1016/j.cub.2017.12.003

SUMMARY

Birds seem to use a light-dependent, radical-pair-based magnetic compass. In vertebrates, cryptochromes are the only class of proteins that form radical pairs upon photo-excitation. Therefore, they are currently the only candidate proteins for light-dependent magnetoreception. Cryptochrome 4 (Cry4) is particularly interesting because it has only been found in vertebrates that use a magnetic compass. However, its structure and localization within the retina has remained unknown. Here, we sequenced night-migratory European robin (*Erithacus rubecula*) *Cry4* from the retina and predicted the currently unresolved structure of the erCry4 protein, which suggests that erCry4 should bind Flavin. We also found that *Cry1a*, *Cry1b*, and *Cry2* mRNA display robust circadian oscillation patterns, whereas *Cry4* shows only a weak circadian oscillation. When we compared the relative mRNA expression levels of the cryptochromes during the spring and autumn migratory seasons relative to the non-migratory seasons in European robins and domestic chickens (*Gallus gallus*), the *Cry4* mRNA expression level in European robin retinae, but not in chicken retinae, is significantly higher during the migratory season compared to the non-migratory seasons. Cry4 protein is specifically expressed in the outer segments of the double cones and long-wavelength single cones in European robins and chickens. A localization of Cry4 in double cones seems to be ideal for light-dependent magnetoreception. Considering all of the data presented here, especially including its localization within the European robin retina, its likely binding of Flavin, and its increased expression during the migratory season in the migratory bird but not in chicken, Cry4 could be the magnetoreceptive protein.

INTRODUCTION

Migratory birds use a magnetic compass for navigation and orientation [1, 2], but the basic sensory mechanisms underlying magnetoreception remain elusive. Strong evidence suggests that the magnetic compass sense in night-migratory birds is light dependent [3] and located in the birds' eyes [4, 5], and that magnetic compass information is processed in a small part of the thalamofugal visual pathway [6–9]. In an extraordinarily far-sighted proposal, Klaus Schulten [10] suggested that hyperfine interactions between electron and nuclear spins combined with Zeeman interactions with the geomagnetic field in molecules generating photo-induced radical pairs could form the basis of a chemical magnetic compass. Since then, this so-called radical-pair mechanism of magnetoreception has come of age, and it is now reasonably well understood how such a mechanism could detect the compass direction of the Earth's magnetic field [7, 11–16]. For the radical pair hypothesis to be relevant for avian magnetoreception, one key requirement is that molecules having the needed biophysical characteristics exist in the eye of migratory birds. The only vertebrate proteins known to form radical pairs upon photoexitation are the cryptochromes [7, 11, 16–19]. Cryptochromes are flavo-proteins that share moderate amino acid similarity to photolyases but do not show photolyase activity [7, 18, 20]. In plants and various animal species, they are involved in blue-light-dependent pathways and in the circadian clock (for a general overview, see [20]). Mammalian cryptochromes involved in the circadian rhythm are mainly localized in cell nuclei [20, 21], whereas magnetoreceptive cryptochromes should be located in the cytosol and be associated with membranes and/or the cytoskeleton [7, 13, 18, 22, 23]. To date, four different cryptochromes have been found in the retina of several bird species [7, 18, 24–31],

Table 1. Amino Acid Residue Numbers for the Conserved Tryptophans W_A, W_B, W_C, W_D in *Arabidopsis thaliana* Cryptochrome 1 (atCry1), *Drosophila melanogaster* Cryptochrome 1 (dmCry1), and *Erithacus rubecula* Cryptochrome 4 (erCry4)

	atCry1	dmCry1	erCry4
W_A	400	420	395
W_B	377	397	372
W_C	324	342	318
W_D	—	395	369

See also Figure S2.

and Cry1a from migratory garden warblers has been shown to form long-lived radical pairs upon photo-excitation [17]. Cry1a is located in the inner and/or outer segments of UV-sensitive photoreceptor cells [25, 26], Cry1b was found in the cytosol of ganglion cells and in the photoreceptor inner segments [29, 30] and Cry2 seems to be widespread and nucleic and is therefore almost certainly a clock protein [25]. Cry4 has been reported to be located in more or less every cell within the retina of domestic chicken and feral pigeons [27, 31], which suggests that Cry4 is either a common housekeeping gene that does not play a highly specific role in a sensory system, or that the antibodies used might have been unspecific. In any case, no information on Cry4 location within the retina of any migratory bird exists. Cry4 is a particularly interesting magnetoreceptor candidate molecule, since (1) it has so far only been found in birds, amphibians, and fish [18, 32, 33], three of the four animal classes in which magnetically guided behavior is particularly well documented [1, 2, 6, 34–37], (2) Cry4 is the only cryptochrome that seems to show no clear endogenous circadian oscillation [38], and (3) it undergoes a light-triggered photocycle involving the formation of a flavosemiquinone radical in chicken [39].

The aims of the present study therefore were (1) to identify the so far unknown sequence of Cry4 of the European robin (*Erithacus rubecula*), (2) to analyze the circadian mRNA expression patterns of all cryptochromes in the retina of European robins, (3) to test whether there are pronounced seasonal differences in the Cry4 expression levels in the night-migratory European robin and/or in the non-migratory domestic chicken (*Gallus gallus*), (4) to explore where Cry4 is located within the retina of European robins, and (5) to predict its currently unknown structure through computational modeling and to use the model to estimate how likely erCry4 is to bind flavin adenine dinucleotide (FAD).

RESULTS

Identification of the Complete Coding Sequence for European Robin Cryptochrome 4

We analyzed the complete Cry4 coding sequence of nine European robins (Figures S1 and S2). These nine sequences showed mismatches at 24 different sites. The mismatches at 21 of these positions are most probably due to polymerase and/or sequencing errors. At nucleotide positions 597, 1014, and 1125, the mismatches occurred in two out of nine individuals and might therefore indicate natural polymorphisms, but all three are synonymous and do not affect the amino acid sequence. The cDNA consensus sequence (deposited under the GenBank accession number KX890129) includes an open reading frame of 1,584 bp encoding a 527-amino-acid protein with an identity of 87.67% to *Gallus gallus* Cry4 protein (GenBank AY300013). European robin Cry4 contains all functional domains characteristic for cryptochrome proteins: the DNA photolyase homology domain, the FAD binding domain, the three or four tryptophans thought to be involved in radical-pair formation (see Table 1), and no nuclear localization sequence.

Circadian Expression Pattern of the Cryptochromes in European Robin Retina

Using qRT-PCR, we found that three of the four retinal cryptochrome transcripts show a pronounced 24-hr rhythm of mRNA expression (Figure 1). The expression pattern of *erCry1a* and *erCry1b* genes displayed a considerable periodicity, with a significant peak in the afternoon (16:00 Central European Time [CET]) and the lowest level at night (between 22:00 and 1:00 CET). For both *erCry1* splice variants, the increase in relative expression is about 7-fold (7.7- and 7.2-fold for *erCry1a* and *erCry1b*, respectively; Tukey-HSD: $p < 0.001$). The mRNA expression pattern of *erCry2* showed a significant out-of-phase oscillation with *erCry1a* and *erCry1b*, with highest expression during the early day (4:00 CET) and lowest in the early afternoon (13:00 CET). The rhythmicity of *erCry2* is weaker than that of *erCry1*, its relative expression increases only 2.9-fold (Tukey-HSD: $p = 0.034$). The statistically significant rhythms of *erCry1a*, *erCry1b*, and *erCry2* were also confirmed by Cosinor analysis ($p < 0.001$ in all cases). For *erCry4*, we did not detect a clear and significant circadian oscillation in European robin retinae (one-way ANOVA: $p = 0.094$). Yet when applying Cosinor analysis, a rhythmical expression of *erCry4* mRNA was found ($p = 0.02$). The reason why the Cosinor analysis finds a slightly significant circadian oscillation in Cry4 is probably the following: if the real expression level at 10:00 CET were at the upper end of the SEM, *erCry4* would show a slightly higher expression value (about 2.5-fold when comparing 22:00 to 13:00 CET) during daytime. In any case, the *erCry4* mRNA levels seem to show a more constant expression profile over the 24-hr period than the other three cryptochromes.

Seasonal Expression Differences of the Cryptochromes

To investigate whether there are differences in mRNA expression levels during the migratory and non-migratory seasons in European robins, we collected eight birds in the non-migratory winter season and compared the relative mRNA expression levels of the cryptochrome genes to those observed in eight birds collected in the migratory seasons (four during autumn and four during spring season), each at 13:00 CET (Figure 2). Both the mRNA of *erCry2* and *erCry4* showed a statistically significantly higher expression level during the migratory seasons (*erCry2* about 1.6 times upregulated, Mann-Whitney test: $p = 0.007$, and *erCry4* about 2.2 times upregulated; Mann-Whitney test: $p = 0.001$). In P1 (postnatal day 1) and P41 non-migratory chickens, we did not find any seasonal expression difference for *ggCry4*. In the P1 chickens, *ggCry1b* seems to be expressed less during spring than during winter season by a factor 0.61 (Mann-Whitney test: $p = 0.009$), but this could be a statistical outlier.

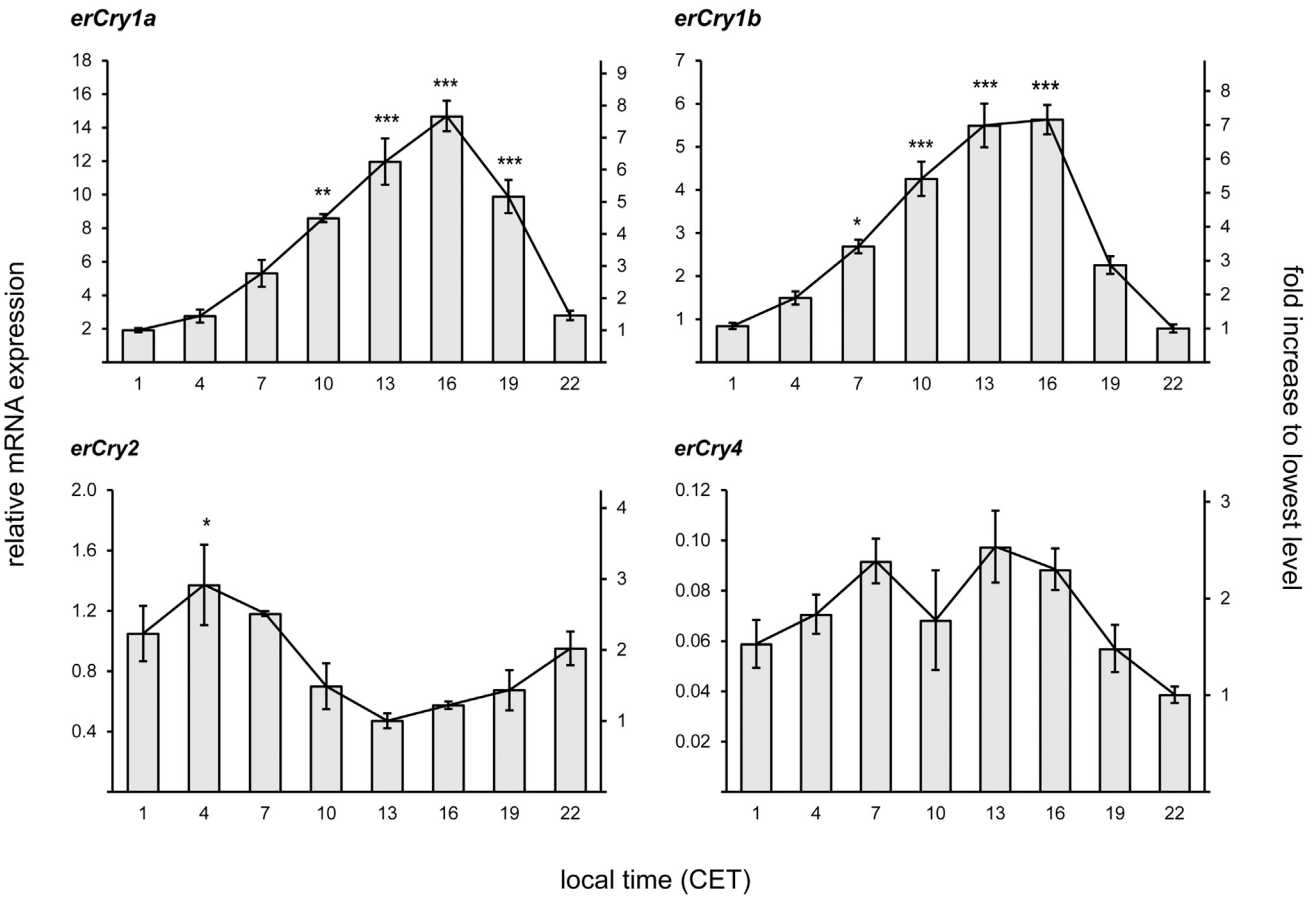


Figure 1. Circadian Expression Profiles for European Robin Retinal Cryptochromes

24-hr profiles were measured in retinal tissue collected at eight time points (local time, CET) during the autumn migratory season. Each bar indicates the relative mRNA expression level normalized to the mRNA levels of the common housekeeping genes *erPrkca*, *erGluR2*, and *erTbp*, which were used as non-circadian reference genes (n = 3, mean values ±SEM; left y axis), and the mRNA amount in relation to the lowest expression value (right y axis). Significant differences at each time point were analyzed by one-way factorial ANOVA, $p < 0.05$; post hoc Tukey HSD test: *$p < 0.05$, **$p < 0.01$, ***$p < 0.001$. Only significant differences relative to the lowest level of mRNA expression of the respective gene are shown. Note the different y axes for each graph. See also Tables S1 and S4.

Localization of *erCry4* within the Retina of European Robins

We generated a custom-made polyclonal antibody specific to a 23-amino-acid peptide at the C-terminal end of the Cry4 protein. The affinity-purified polyclonal Cry4 antibody was highly specific for the Cry4 protein (see the ''Controls and antibody specificity'' section below) and indicated a highly distinct immunoreactivity in some but not all photoreceptor outer and inner segments of twelve European robins (eight collected during the migratory seasons and four collected during the non-migratory seasons; Figure 3B, green). We observed no consistent seasonal variation. In a previous study, Watari and colleagues [27] reported that Cry4 protein is located in more or less every cell type of the chicken retina. Their antibody, albeit directed against the same epitope region, recognized a shorter region than our antibody did. To exclude species-specific differences of the Cry4 immunosignal between very remotely related domestic chickens and European robins, we also stained three retinae from chickens. Our polyclonal Cry4 antibody showed the same immunoreactivity pattern in the chickens as in the European robins (Figure 3D, green). To find out in which photoreceptor type(s) Cry4 is located, we performed immunohistochemical double stainings with the polyclonal Cry4 antibody (Figure 4, green) combined with different opsin antibodies (Figure 4, magenta). The Cry4 antibody signal was always found in the same outer segments as the iodopsin antibody signal (Figures 4B and 4C). In contrast, double stainings with the Cry4 antibody and antibodies against the short wavelength opsin (UVopsin, Figures 4E and 4G), blue opsin (Figures 4M and 4O), and rhodopsin (Figures 4I and 4K) always showed non-overlapping signals in different photoreceptor outer segments. In birds, iodopsin is expressed exclusively in long-wavelength single cones and in double cones [40, 41]. Since all Cry4-stained outer segments were also iodopsin positive, Cry4 is expressed in the outer segments of both double cones and long-wavelength single cones. The inner segments of double cones express calbindin [42]. Double staining with Cry4 and calbindin antibodies confirmed that Cry4 is located in the double cones and long-wavelength single cones (Figure 5). We found the

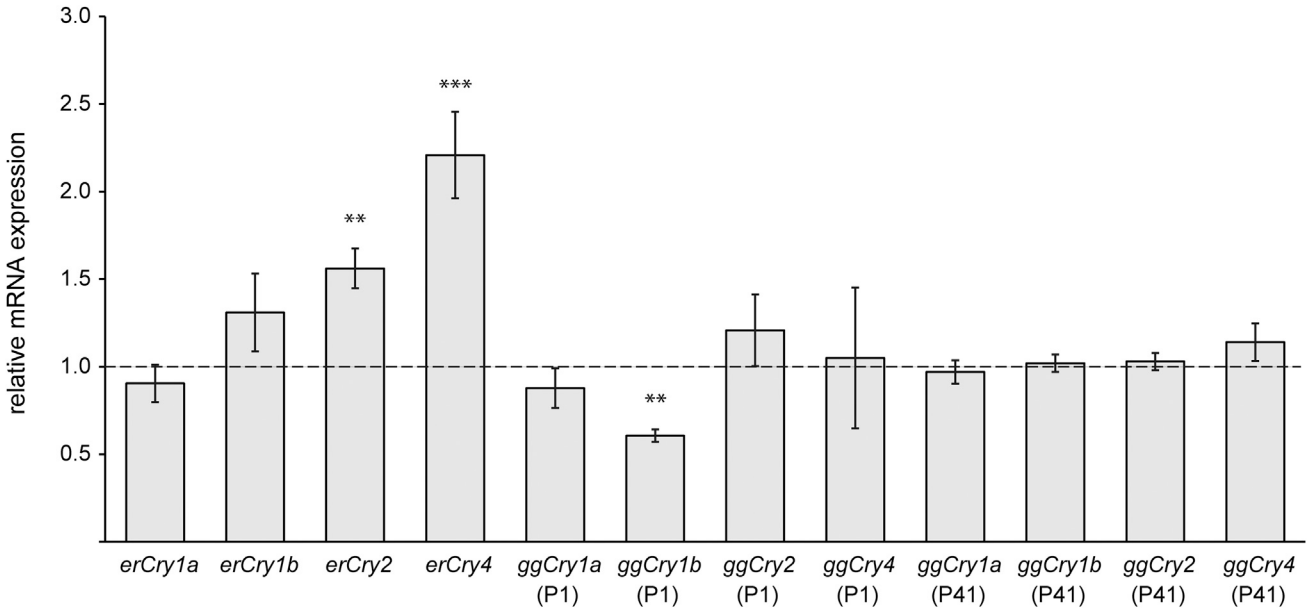


Figure 2. Relative Expression of the Cryptochromes of European Robins and Chickens in Retinae Collected during the Migratory Autumn/Spring Seasons Relative to the Expression during the Non-migratory Winter/Summer Seasons

A value of 1 indicates the same level of expression in both seasons (n = 8+8 for European robins, 6+6 for chickens P1, and 4+4 for chickens P41; mean values ± SEM are shown). A significant expression difference between autumn/spring seasons in comparison to winter/summer seasons was tested using the Mann-Whitney test, **p < 0.01, ***p = 0.001. See also Tables S1, S2, and S4.

described staining pattern in all parts of all the studied retinas, from the periphery to the center and from dorsal to lateral. We also observed that the number of Cry4-positive cones is a factor 4.86 ± 0.77 (SD) more abundant than the UV cones. The approximate frequency of the different cone types in birds (chicken) is known: 20% rods, 32% double cones, 17% green single cones, 14% long-wavelength (red) single cones, 10% blue single cones, and 7% UV single cones [41]. Therefore, the finding that our polyclonal Cry4 antibody co-localizes with iodopsin and stains many more photoreceptor cell outer segments than the antibodies against rhodopsin, UV opsin and blue opsin did, fits well with these abundances. A monoclonal erCry4 antibody subsequently developed indicated exactly the same immunoreactivity pattern as the polyclonal Cry4 antibody did in retina slices from the same five individual European robins (Figure 6A). Double stainings with the UVopsin antibody (Figure 6B, magenta) indicated that UVopsin is not located in the same cells as Cry4. Double staining of the monoclonal erCry4 antibody with the other opsin antibodies was not possible since all these antibodies had been manufactured in rodents and the secondary antibodies against mouse cross-reacted with the monoclonal antibodies from rat and vice versa.

Controls and Antibody Specificity

To test the specificity of the two Cry4 antibodies, we did a large number of control experiments, as proposed by the International Working group for antibody validation (IWGAV) [43]. First, we obtained no antibody signal when exchanging the polyclonal Cry4 antibody with the pre-immune serum (Figures S3A and S3B, green) or when pre-adsorbing the antibody with the antigenic peptide (Figures S3C and S3D, green). Second, in western blots, the polyclonal Cry4 antibody identified a protein of the expected molecular mass in both total homogenate of European robin retina (approximately 61 kDa, Figure S4M) and in protein homogenates of recombinant erCry4-GFP-expressing COS-1 cells (approximately 89 kDa, Figure S4M). The signal from the polyclonal Cry4 antibody was absent in negative controls after stripping and re-probing the blot with pre-immune serum and after pre-adsorbing with the Cry4 immunization peptide (Figures S4N and S4O). Third, we tested the polyclonal Cry4 antibody for cross-reactivity with erCry1a, erCry1b, and erCry2 by generating COS-1 cells expressing recombinant Cry-GFP fusion proteins. The green fluorescence of the COS-1 cells expressing the erCry4-GFP fusion protein was co-localized with the magenta Cry4 antibody staining, confirming that the antibody detects the erCry4 protein (Figures S4A–S4C). In contrast, we detected no Cry4 antibody signal on COS-1 cells expressing recombinant erCry1a-GFP, erCry1b-GFP, or erCry2-GFP fusion proteins, respectively (Figures S4D–S4L). Thus, the polyclonal Cry4 antibody exhibits no cross-reactivity with other known cryptochrome proteins. By replacing the polyclonal Cry4 antibody with pre-immune serum or omitting it, we could exclude cross-reactions of erCry4-GFP-expressing cells with antibodies present before immunization of the guinea pig and with the secondary antibody (Figures S5A–S5F). When the polyclonal Cry4 antibody was pre-adsorbed with the Cry4 immunization peptide, we detected no staining on erCry4-expressing cells, which confirms that the polyclonal Cry4 antibody recognizes specific epitopes on the peptides used for immunization (Figures S5G–S5I). The monoclonal erCry4 antibody showed no immunosignal on retinal slices when being pre-adsorbed with the antigenic peptide (Figures 6C and 6D, green). In western blots, the

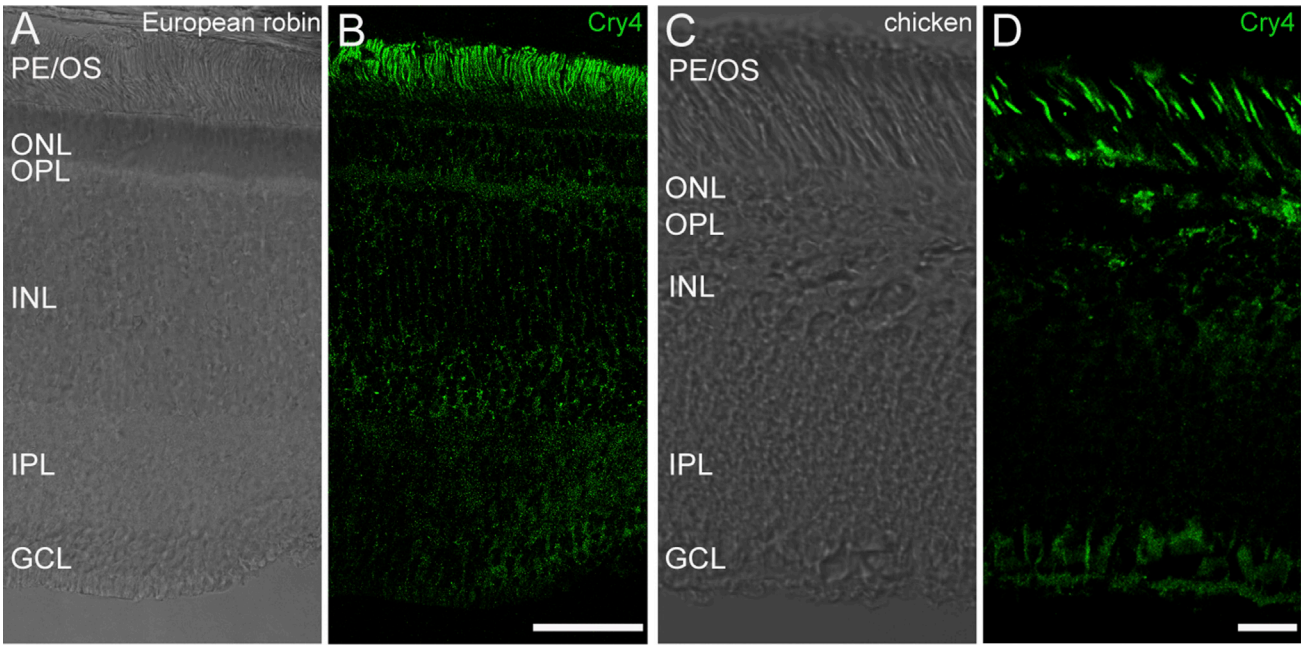


Figure 3. Cry4 Is Expressed in the Outer Segments of Specific Photoreceptor Cells in the Retina of European Robin and Chicken

Vertical slices of European robin (A and B) and chicken (C and D) retina labeled with the polyclonal Cry4 antibody. With the bright-field image for comparison (A and C), Cry4 immunoreactivity (B and D, green) was located in the cytoplasm of specific photoreceptor outer segments. All images are single confocal images (not stacks) with identical microscope settings. Scale bars in (B) and (D), 50 μm. PE, pigment epithelium; OS, photoreceptor outer segments; ONL, outer nuclear layer; OPL, outer plexiform layer; INL, inner nuclear layer; IPL, inner plexiform layer; GCL, ganglion cell layer. See also Figures S3–S5.

monoclonal erCry4 antibody detects a band of the expected size in the retinal homogenate of European robin and in the lysate of erCry4-GFP-expressing COS-1 cells, but not in a lysate of COS-1 cells exclusively expressing GFP (Figure 6N). Stainings of COS-1 cells that expressed erCry1a-GFP, erCry1b-GFP, and erCry4-GFP fusion proteins showed that the monoclonal erCry4 antibody did not cross-react with other known cryptochromes in transfected cells (Figures 6E–6M). Since we had produced the monoclonal antibodies against gglodopsin and ggBlueOpsin for this study, we also tested their specificity by generating HEK293 cells expressing all five chicken opsins as GFP-fusion proteins (Figures S6 and S7). The antibodies against iodopsin (Figure S6) and ggBlueOpsin (Figure S7) exclusively stained the cells expressing gglodopsin-GFP (Figures S6N and S6O) and ggBlueOpsin-GFP proteins (Figures S7H and S7I), respectively. This shows that neither the gglodopsin nor the ggBlueOpsin antibody exhibit any cross-reactivity with other opsin proteins occurring in the eyes of chicken or with the GFP protein expressed in HEK293 cells.

Structural Model of erCry4

Kutta and colleagues suggested that vertebrate cryptochromes do not bind FAD [44]. Since there are currently no crystal structures available for any Cry4 or for any bird cryptochrome, we used homology modeling combined with extensive molecular dynamics (MD) simulations to predict the structure of the photolyase homology region (PHR) domain of erCry4 (Figure 7). We used the model to evaluate the likelihood of FAD binding and the exact positions of the FAD and the tryptophan triad, which are essential for the radical-pair mechanism. Kutta et al. [44] suggested that R237, R298, Q311, and N419 are important for FAD binding in dmCry. Alignment of the sequences of erCry4 and dmCry suggests that erCry4 possesses the amino acids H222, P281, Q287, and N394 in those locations. However, the modeled structure of erCry4 reveals that R236 is in the same location as the R298 in dmCry (Figure 7E). This means that three of the four important amino acids suggested by Kutta et al. [44] seem to be conserved. Furthermore, R236 seems to be located even closer to FAD in erCry4 than R298 is in dmCry, indicating stronger FAD binding by forming two hydrogen bonds between R236 and the pyrophosphate of FAD, with the average O…H distance of ~1.8 Å. Thus, the suggested interaction between FAD and R298, mediated by a water molecule, in dmCry [44] seems to be absent in erCry4. Through double mutations of R298 and Q311 in dmCry, Kutta et al. have identified these two amino acids as being important for FAD binding. The modeled structure of erCry4 suggests that these amino acids are conserved, which speaks for FAD binding in erCry4. Structural comparison of amino acids surrounding the isoalloxazine part of the FAD in atCry1, dmCry1, and erCry4 reveals that atCry1 features a serine at position 366 where both dmCry1 and erCry4 have an alanine (A385 and A360, respectively; Figure 7D). Furthermore, atCry1 possesses an aspartic acid at position 396, which has been suggested to play an important role in the photoactivation process of plant cryptochrome [45, 46]. The aspartic acid is replaced by an asparagine (N391) in erCry4. Last, atCry1 has a valine at position 363 (V363) where dmCry1 features an asparagine (N382) and erCry4 has a histidine (H357). Concerning the tryptophan triad, the modeled structure of erCry4 indicates that the positions of FAD, W_A, and W_B are similar in the three different proteins.

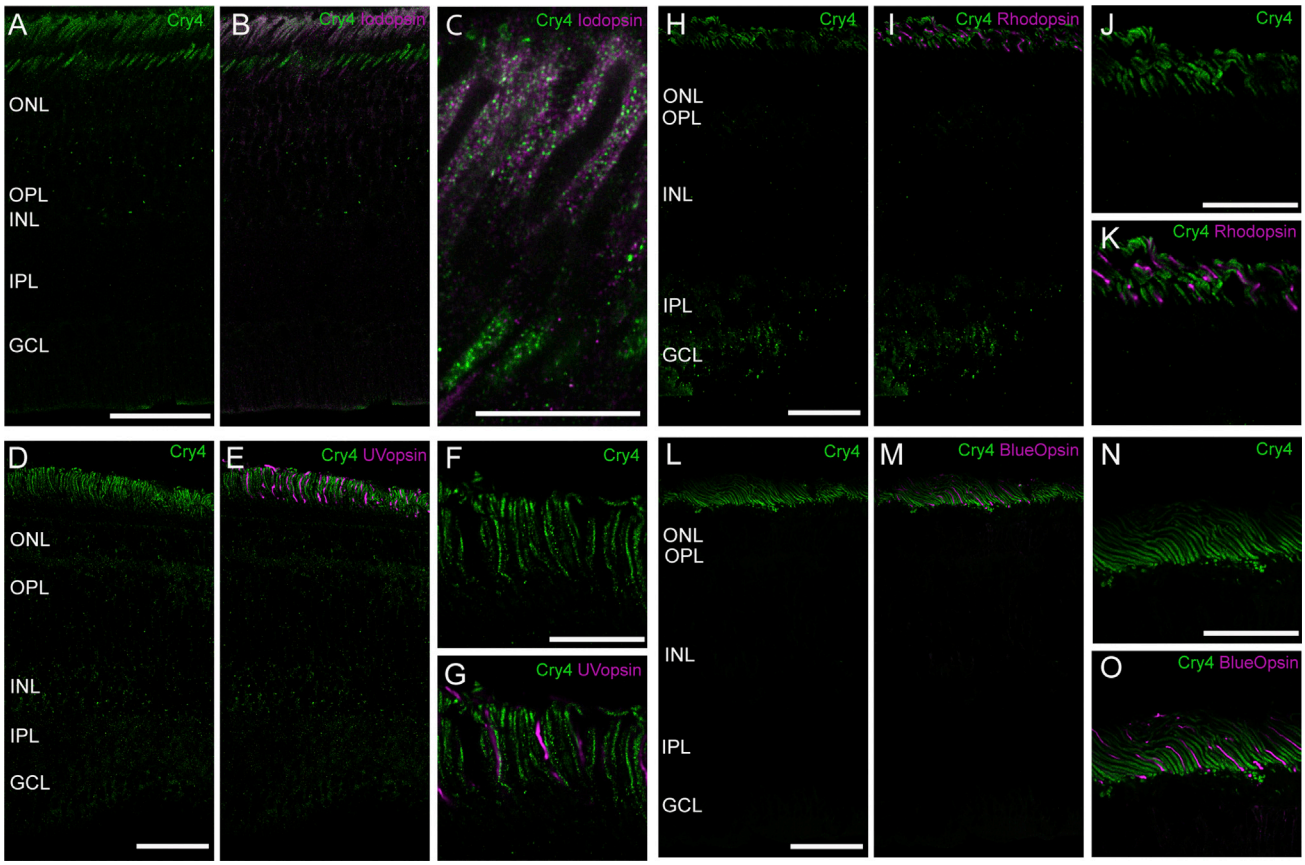


Figure 4. Cry4 Is Expressed in the Outer Segments of Double Cones and Long Wavelength Single Cones in the European Robin Retina

Vertical slices of European robin retinae labeled with the polyclonal Cry4 antibody (green) showed a strong expression of Cry4 protein in the outer segments of some but not all photoreceptor cells. Iodopsin (B and C), UVopsin (E and G), rhodopsin (I and K), and blue opsin antibody (M and O) were expressed in outer segments and inner segments of double and long-wavelength single cones, UV cones, rods, and blue cones, respectively. A closer look at the Cry4 labeling (C, green) together with a iodopsin antibody (C, magenta) showed that Cry4 is expressed in the same outer segments as iodopsin. A closer look at the double stainings of the polyclonal Cry4 antibody with UVopsin (G, magenta), rhodopsin (K, magenta), and blue opsin antibody (O, magenta) showed that the signals are not localized in the same cells. For illustration purposes, all images were enhanced in brightness. Scale bars in (A), (D), (H), and (L), 50 μm, in (C), 10 μm, and in (F), (J), and (N), 25 μm. (C), (F), (G), (K), (N), and (O) are enlargements of parts of the corresponding whole-retinal images.

However, the position and orientation of W_C is similar only for dmCry1 and erCry4, while atCry1 shows a different positioning of the W_C residue (residue numbers listed in Table 1, see also Figure S2B). The fourth tryptophan, W_D, relevant for cryptochrome activation [47], is present in both dmCry and erCry4 and preserves its position (Figure 7B). Most other parts of the proteins are highly similar, except for two differences (see Figure 7C).

DISCUSSION

Daily Variation of Retinal Cryptochrome mRNA Expression

Our 24-hr expression profiles of *Cry1* and *Cry2* in the European robin retina are similar to previous observations in birds. The two avian *Cry1* splice variants *Cry1a* and *Cry1b* have, with the exception of the study of Fusani and colleagues [28], not been investigated separately but only as pooled *Cry1* mRNA. Here, we find that both *Cry1a* and *Cry1b* mRNA expression levels exhibit robust and synchronous periodicity with highest expression in the afternoon and lowest expression at night, which is in agreement with the expression profiles found for *Cry1* in other bird species [38, 48–52]. At first glance, the current expression profiles seem to contrast the data from Mouritsen et al. [25], who observed more Cry1 protein in the eye of migratory garden warblers (*Sylvia borin*) at night than during the day. However, Mouritsen et al. [25] looked at protein levels, whereas our present data are based on mRNA expression levels. The differences might therefore result from the time it takes to translate, transport, and accumulate the functional protein at its destined location. The expression patterns of *Cry1a* and *Cry1b* we found do not agree with the results from Fusani et al. [28], who reported higher *Cry1a* and *Cry1b* mRNA expression at night (22:00 CET; 3 hr after lights off) than at day (10:00 CET; 3 hr after lights on) in the eye of night-migratory blackcaps (*Sylvia atricapilla*). The results of Fusani et al. [28] are in disagreement not only with our present results, but also with many other studies of the expression profiles of *Cry1* in other bird species [38, 48–52]. The retinal localization of Cry1b protein has recently been characterized in the European robin and pigeon [29, 30].

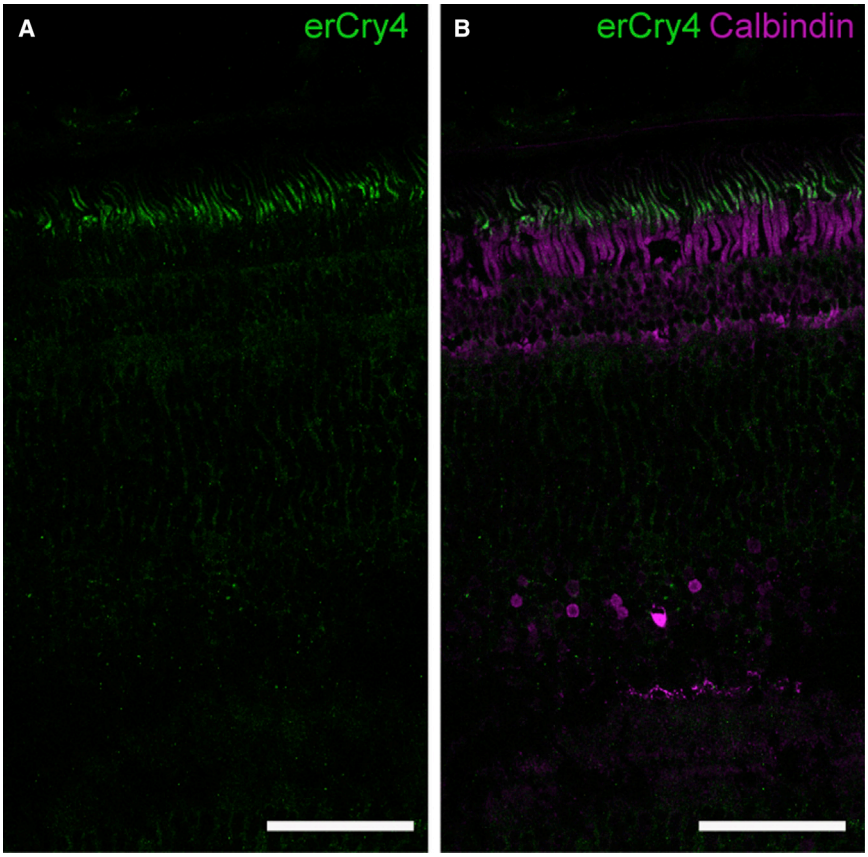


Figure 5. The Polyclonal Cry4 Antibody Signal Is Located in the Outer Segments of Calbindin-Labeled Double Cones

Vertical slices of European robin retinae labeled with the polyclonal Cry4 antibody (A and B, green) and a calbindin antibody (B, magenta). Cry4 is located in the outer segment of all the calbindin-positive cells, thus confirming that the Cry4-labeled cells are primarily the double cones. The Cry4 antibody also labeled a few outer segments of photoreceptor cells that did not seem to have a calbindin-positive inner segment. These are long-wavelength single cones. The images are single confocal images (not stacks) with identical microscope settings. Scale bars, 50 μm.

Cry1b possesses a unique C terminus so far exclusively found in birds. Based on this, a specialized, potential non-clock function has been suggested for Cry1b protein [29]. In our present study, *Cry1b* mRNA expression shows an equally robust circadian rhythmicity as *Cry1a*. This seems to speak against a role of Cry1b in magnetoreception and instead suggests an involvement in circadian clock regulation. For *Cry2* mRNA expression, our results demonstrate a significant circadian rhythmicity, albeit out-of-phase and at lower amplitudes than *Cry1a* and *Cry1b* mRNA. *Cry2* expression peaks at night and reaches its minimum at mid-day. This is consistent with previous findings from the retina [52, 53], brain [48], and pineal gland [38, 53] of other bird species and strongly supports a role of avian Cry2 as a circadian clock protein. In contrast to *Cry1a*, *Cry1b*, and *Cry2* expression, the mRNA of *Cry4* does not seem to fluctuate as clearly over a 24-hr period. This agrees with findings from the chicken retina [38] and the house sparrow brain [48]. The lack of considerable daily oscillation makes it rather unlikely that erCry4 plays a role in the circadian clock.

Seasonal Differences of Cry4 mRNA Expression in European Robin Retina

When comparing the mRNA expression levels of the cryptochromes in retinae collected during the migratory and non-migratory seasons at 13:00 CET, we find that the mRNA of *erCry4* is significantly upregulated during the migratory season. In contrast, *Cry4* expression in non-migrating chickens shows no seasonal differences, neither in P1 nor in P41 chickens. Magnetic compass orientation has been reported for non-migrating birds such as pigeons [1, 2]. Nevertheless, the seasonal differences we observe for *erCry4* in a night-migratory bird might be a hint for Cry4 involvement in magnetoreception, as it seems plausible that the expression level of a magnetic detector protein could be higher during the migratory phase than during the sedentary phase. Moreover, we do not detect any seasonal upregulation of *erCry1b* mRNA. This is in disagreement with Niessner et al. [30], who claimed—based on a very small sample size— that erCry1b protein is only strongly expressed during the migratory period. The present findings confirm what we already pointed out in our parallel paper [29]: there are no pronounced seasonal differences in erCry1b expression. We also detected a slight upregulation of *erCry2* in the European robins during the migratory season and a slight downregulation of *ggCry1b* gene expression in spring in P1 but not P41 chickens. The latter two observed expression differences could be due to chance effects.

Localization of Cry4 within the Retina of European Robins

The basic requirement for reliable results in immunohistochemistry is the specific binding of the antibody to the antigenic peptide. Since we did not have the option of creating knockout animals (a knockout migratory bird has never been generated), we compensated by performing many control procedures as proposed in the guidelines for proper controls in immunohistochemical experiments [43, 54]. We are therefore confident that our Cry4 antibodies specifically detected the erCry4 protein. Two studies [27, 31] previously reported that Cry4 protein is expressed more or less in every cell type within the retina of domestic chickens and feral pigeons, respectively. When an antibody stains more or less all cell types in the retina, the target protein is either a common housekeeping gene involved in very basic cell functions (such as IscA1, beta-actin, and various clock proteins), which do not play a highly specific role in a sensory system, or the antibody is not very specific (see also [55]). If Cry4 is part of a magnetic sensory system, we would expect it to be

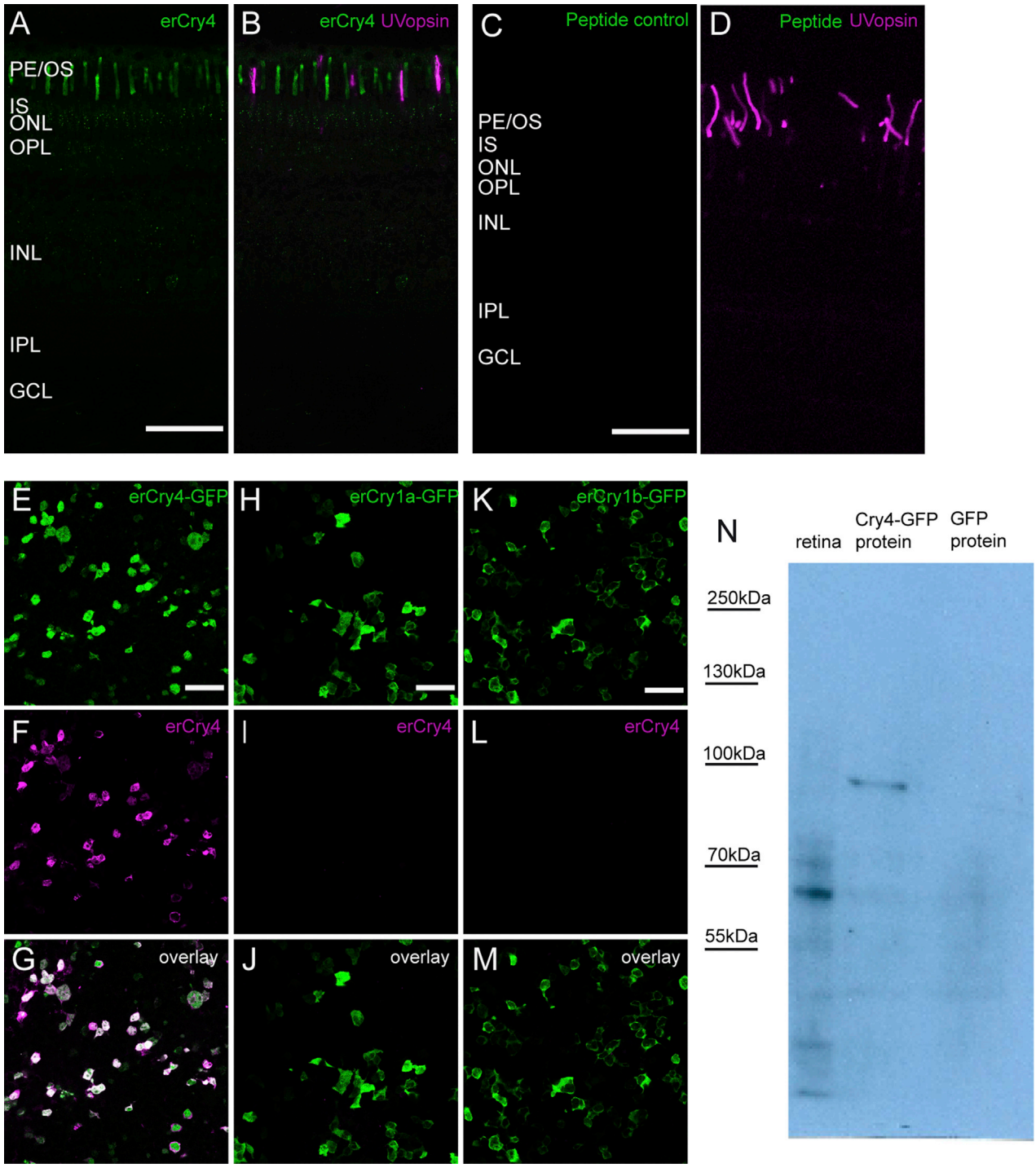


Figure 6. Like the Polyclonal Cry4 Antibody, the Monoclonal erCry4 Antibody Stains the Outer Segments of Specific Photoreceptor Cells in the European Robin

Vertical slices of European robin retinae labeled with the monoclonal erCry4 antibody (A and B, green) and short wavelength opsin antibody (B, magenta). The Cry4 staining was absent when pre-incubating the erCry4 monoclonal antibody with the immunization peptide (C and D, green). COS-1 cells expressing an erCry4-GFP fusion protein (E, green) stained with the monoclonal erCry4 antibody (F, magenta) indicated that the antibody detects erCry4-GFP-expressing cells (G, white). The same labeling of erCry1a-GFP (H–J) or erCry1b-GFP (K–M)-expressing cells indicated no cross-reaction between the monoclonal erCry4 antibody and other cryptochromes. In western blotting, the monoclonal erCry4 antibody detected a band at the expected size of the erCry4-GFP protein complex (89 kDa) in lysates of erCry4-GFP-expressing COS-1 cells (N, middle lane). This band is missing in lysates of COS-1 cells only expressing GFP (N, right lane). In the European robin total retina homogenate, the monoclonal erCry4 antibody detected a weak band at the expected erCry4 protein size of 61 kDa (N). The remaining very faint bands in the blots could be proteolytic degradation products. For illustration, images (A)–(D) are adjusted in brightness. Scale bars, 50 μm. See also Figures S6 and S7.

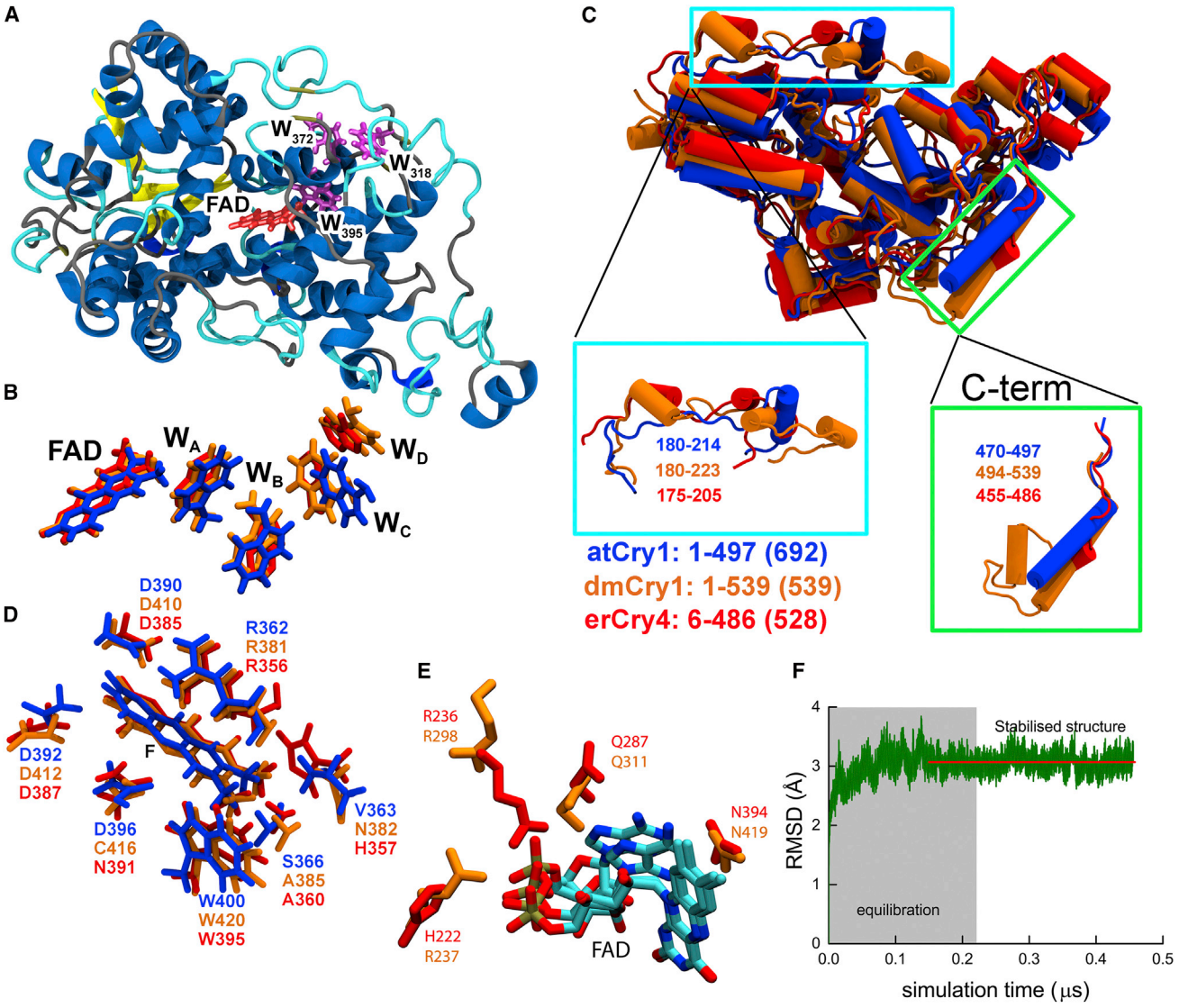


Figure 7. Equilibrated Structural Model of erCry4

(A) The secondary structure of the erCry4 model obtained after extensive MD equilibration, with the isoalloxazine part of the FAD (red) and the conserved tryptophan triad (magenta).

(B) Superimposed molecular structures of the FAD isoalloxazine part and the tryptophan triad from atCry1 (blue), tetrad from dmCry1 (orange), and the tetrad from erCry4 model (red).

(C) Structural alignment of atCry1 (blue), dmCry1 (orange), and the erCry4 model (red), suggesting two major structural differences in the three proteins: (1) the surface-exposed parts of the proteins feature one large helix in atCry1, whereas dmCry1 and the erCry4 model feature three and two smaller helices respectively (blue box), and (2) atCry1 and dmCry1 feature one helix at the end of the PHR domain, while the erCry4 model features a shorter helix in the same structural area (green box). One reason for this discrepancy might be that dmCry1 is the only cryptochrome where the C terminus is resolved in the crystal structure, whereas the atCry1 structure and the erCry4 model only include the PHR domain. To include the complete structure of atCry1 and erCry4 would change the C-terminal part, which, unfortunately, cannot be predicted reliably yet.

(D and E) Comparison of the amino acid residues surrounding the FAD in the binding pocket of atCry1 (D) and dmCry1 and erCry4 (D and E).

(F) Homology models of proteins obtained directly from web servers can rarely be used as reliable structures for further analysis since these models are usually not stabilized. The stability of the homology model can be established and probed by MD simulations, as done here for the model of erCry4. (F) shows the root-mean-square deviation (RMSD) of the protein backbone atoms computed relatively to the initial structure of the model for erCry4 during the entire 0.5-μs MD simulation performed on our erCry4 model. The gray area indicates the equilibration interval, while the remaining simulation was used to justify the stability of the model (production simulation).

See also Figures S1 and S2.

located only in cells being part of a specific sensory pathway. Furthermore, Watari and co-workers [27] show an exclusively nucleic staining, whereas it is difficult to say what the staining of Qin and colleagues [31] really shows, because their DAPI staining does not seem to be purely nucleic and it looks as if their Cry4 staining is at least partly nucleic. However, Cry4 has no

nuclear localization sequence. If Cry4 would indeed be nucleic, it would probably function as a transcription factor, e.g., as a clock protein. In summary, we assume that the antibodies used in these two previous studies [27, 31] were unspecific [55]. Due to the specificity of our antibodies and the large phylogenetic separation of chickens and European robins, it is likely that the localization of Cry4 in the outer segments of double cones and long wavelength single cones we observed will be found in most bird species.

The retinal localization pattern we discovered suggests that Cry4 fulfills a specialized function in a specific sensory pathway. Since the cryptochromes are currently the only class of vertebrate proteins known to form radical pairs upon photo-excitation [7, 11, 13, 17–19], Cry4 could be a magnetoreceptive protein. Its location in the outer segments of the double cones makes Cry4 an even likelier magnetoreception candidate, because the hundreds of parallel cell membranes in photoreceptor outer segments would facilitate an at least partial alignment of the cryptochromes relative to one another [7, 18, 22, 23, 26], and a magnetic compass sensor most likely require the correlated responses of many radical pairs. Furthermore, despite the fact that ~32% of the photoreceptor cells in many birds are double cones [41], their function is not completely clear [41, 56]. It has been suggested that, especially if the cryptochromes and/or opsins are orthogonally oriented in the two sub-cones, they would be particularly well suited for light-dependent magnetoreception and/or polarized light detection for the following reasons [7]: since the first step in light-dependent magnetoreception is light detection, not magnetoreception, a change in light intensity would have the same effect on a receptor cell as a change in the magnetic stimulus if we consider a single light-dependent magnetoreceptor cell in isolation [7, 23]. This is analogous to the situation in color vision, where a single color receptor cannot determine whether an increased activation is due to a general increase of light intensity or a change in color [7]. Color vision is achieved by comparing the responses of two neighboring receptors that are sensitive to different parts of the visual spectrum [57]. In a similar fashion, the separation of light and magnetic field effects could most elegantly be realized by having two populations of identical receptor molecules with identical spectral absorption characteristics in close proximity to each other, but with different, ideally perpendicular, orientations in neighboring cells, e.g., double cones [7]. Due to their close spatial proximity, their light input will usually be the same, whereas the magnetic field effects would be different. The recent finding of parallel rhodopsin dimer tracks oriented parallel to the outer disk incisures in mouse rods under low light conditions [58] and geometrical considerations [59] add some credibility to this speculative suggestion. Comparison of the outputs of the two receptor populations could be achieved in the early stages of neuronal processing and the resulting signal could then be processed in a specialized neuronal information channel dedicated to magnetic sensing separate from image formation processing (see illustration of this idea in [7]).

Modeled erCry4 Structure

Our structural predictions suggest that erCry4 will bind FAD. Furthermore, the equilibrated putative structure of Cry4, proposed here, could be used to calculate possible magnetic field effects and compare those with magnetic field effects in plant (atCry1) and insect (dmCry1) cryptochromes, where magnetic field effects have been documented earlier [60, 61]. This might contribute to our understanding of radical-pair-based magnetoreception.

Conclusions

We have documented that Cry4 is very strongly expressed in the outer segments of double cones and long wavelength single cones all over the retina of European robin and chicken and that Cry4 is more strongly expressed during the migratory season than during the non-migratory season in the night-migratory European robins. Even though there is no clear evidence showing which of the four cryptochromes—if any—is the primary magnetoreceptor in night-migratory songbirds, several properties of erCry4 indicate that it differs from other cryptochromes. So far, Cry4 has only been found in species showing magnetoreceptive behavior, and there are no indications that it operates as a clock protein in the control of circadian rhythms. Our study further suggests that erCry4 is probably going to bind FAD and that erCry4 is expressed at the seemingly most suitable location to be a primary, light-dependent, radical-pair-based magnetoreceptor in birds. This makes Cry4, in our opinion, the most likely magnetoreceptor candidate among the cryptochromes.

STAR★METHODS

Detailed methods are provided in the online version of this paper and include the following:

- KEY RESOURCES TABLE
- CONTACT FOR REAGENT AND RESOURCE SHARING
- EXPERIMENTAL MODEL AND SUBJECT DETAILS
- METHOD DETAILS
  - Amplification and identification of the cDNA sequences
  - Quantitative reverse transcriptase polymerase chain reaction
  - Antibody generation
  - Immunohistochemistry
  - Cell culture and protein expression
  - Immunocytochemistry of transfected cells
  - Western blot analysis
  - Confocal microscopy
  - Computational modeling
- QUANTIFICATION AND STATISTICAL ANALYSIS
- DATA AND SOFTWARE AVAILABILITY

SUPPLEMENTAL INFORMATION

Supplemental Information includes seven figures and six tables and can be found with this article online at https://doi.org/10.1016/j.cub.2017.12.003.

ACKNOWLEDGMENTS

We thank Karin Dedek, Arndt Meyer, Margrit Kanje, Irina Formins, and Beate Grünberg for technical support in the lab and advice and Dmitry Kobylkov for help with statistics. We also thank Florian Bleibaum for the design and production of the pTurboGFP-N vectors coding for *erCry1a* and *erCry1b* and Sina Engler for providing the pTurboGFP-N vector coding for *erCry2*. This project was funded by the DFG (FOR701 and MO 1408/1-2 to H.M. and GRK 1885 to A.E., H.M., and K.-W.K.), a Lichtenberg Professorship from

the Volkswagen Stiftung to H.M., the Air Force Office of Scientific Research (Air Force Materiel Command USAF award FA9550-14-1-0095 to H.M. and K.-W.K.), and the Lundbeck Foundation to I.A.S. Computational resources for the work described in this paper were supported by the DeiC National HPC Center, SDU.

AUTHOR CONTRIBUTIONS

Experiment Design and Supervision, H.M., I.A.S., K.-W.K., P.B., A.E., A.G., and E.S.; Experiments, A.G., A.E., and E.S.; Data Analysis, A.E., A.G., E.S., I.A.S., and H.M.; Monoclonal Antibody Generation, R.F.; Writing, A.G., A.E., H.M., E.S., I.A.S., K.-W.K., and P.B.

DECLARATION OF INTERESTS

The authors declare no competing interests.

Received: October 14, 2017
Revised: November 24, 2017
Accepted: December 2, 2017
Published: January 4, 2018

REFERENCES

1. Wiltschko, R., and Wiltschko, W. (1995). Magnetic Orientation in Animals (Zoophysiology Volume 33) (Springer).
2. Mouritsen, H. (2013). The magnetic senses. In Neurosciences – From Molecule to Behavior: A University Textbook, C.G. Galizia, and P.M. Lledo, eds. (Springer), pp. 427–443.
3. Wiltschko, W., Munro, U., Ford, H., and Wiltschko, R. (1993). Red light disrupts magnetic orientation of migratory birds. Nature *364*, 525–527.
4. Hein, C.M., Zapka, M., Heyers, D., Kutzschbauch, S., Schneider, N.L., and Mouritsen, H. (2010). Night-migratory garden warblers can orient with their magnetic compass using the left, the right or both eyes. J. R. Soc. Interface *7* (*Suppl 2*), S227–S233.
5. Hein, C.M., Engels, S., Kishkinev, D., and Mouritsen, H. (2011). Robins have a magnetic compass in both eyes. Nature *471*, E11–E12, discussion, E12–E13.
6. Zapka, M., Heyers, D., Hein, C.M., Engels, S., Schneider, N.L., Hans, J., Weiler, S., Dreyer, D., Kishkinev, D., Wild, J.M., and Mouritsen, H. (2009). Visual but not trigeminal mediation of magnetic compass information in a migratory bird. Nature *461*, 1274–1277.
7. Hore, P.J., and Mouritsen, H. (2016). The radical-pair mechanism of magnetoreception. Annu. Rev. Biophys. *45*, 299–344.
8. Heyers, D., Manns, M., Luksch, H., Güntürkün, O., and Mouritsen, H. (2007). A visual pathway links brain structures active during magnetic compass orientation in migratory birds. PLoS ONE *2*, e937.
9. Mouritsen, H., Heyers, D., and Güntürkün, O. (2016). The neural basis of long-distance navigation in birds. Annu. Rev. Physiol. *78*, 133–154.
10. Schulten, K., Swenberg, C.E., and Weller, A. (1978). A biomagnetic sensory mechanism based on magnetic field modulated coherent electron spin motion. Z. Phys. Chem. (N. F.) *11*, 1–5.
11. Ritz, T., Adem, S., and Schulten, K. (2000). A model for photoreceptor-based magnetoreception in birds. Biophys. J. *78*, 707–718.
12. Engels, S., Schneider, N.L., Lefeldt, N., Hein, C.M., Zapka, M., Michalik, A., Elbers, D., Kittel, A., Hore, P.J., and Mouritsen, H. (2014). Anthropogenic electromagnetic noise disrupts magnetic compass orientation in a migratory bird. Nature *509*, 353–356.
13. Solov'yov, I.A., Ritz, T., Schulten, K., and Hore, P.J. (2014). A chemical compass for bird navigation. In Quantum Effects in Biology, M. Mohseni, Y. Omar, G. Engel, and M.B. Plenio, eds. (Cambridge University Press), pp. 218–236.
14. Hiscock, H.G., Worster, S., Kattnig, D.R., Steers, C., Jin, Y., Manolopoulos, D.E., Mouritsen, H., and Hore, P.J. (2016). The quantum needle of the avian magnetic compass. Proc. Natl. Acad. Sci. USA *113*, 4634–4639.
15. Maeda, K., Henbest, K.B., Cintolesi, F., Kuprov, I., Rodgers, C.T., Liddell, P.A., Gust, D., Timmel, C.R., and Hore, P.J. (2008). Chemical compass model of avian magnetoreception. Nature *453*, 387–390.
16. Giovani, B., Byrdin, M., Ahmad, M., and Brettel, K. (2003). Light-induced electron transfer in a cryptochrome blue-light photoreceptor. Nat. Struct. Biol. *10*, 489–490.
17. Liedvogel, M., Maeda, K., Henbest, K., Schleicher, E., Simon, T., Timmel, C.R., Hore, P.J., and Mouritsen, H. (2007). Chemical magnetoreception: Bird cryptochrome 1a is excited by blue light and forms long-lived radical-pairs. PLoS ONE *2*, e1106.
18. Liedvogel, M., and Mouritsen, H. (2010). Cryptochromes–a potential magnetoreceptor: What do we know and what do we want to know? J. R. Soc. Interface *7* (*Suppl 2*), S147–S162.
19. Maeda, K., Robinson, A.J., Henbest, K.B., Hogben, H.J., Biskup, T., Ahmad, M., Schleicher, E., Weber, S., Timmel, C.R., and Hore, P.J. (2012). Magnetically sensitive light-induced reactions in cryptochrome are consistent with its proposed role as a magnetoreceptor. Proc. Natl. Acad. Sci. USA *109*, 4774–4779.
20. Sancar, A. (2003). Structure and function of DNA photolyase and cryptochrome blue-light photoreceptors. Chem. Rev. *103*, 2203–2237.
21. Kume, K., Zylka, M.J., Sriram, S., Shearman, L.P., Weaver, D.R., Jin, X., Maywood, E.S., Hastings, M.H., and Reppert, S.M. (1999). mCRY1 and mCRY2 are essential components of the negative limb of the circadian clock feedback loop. Cell *98*, 193–205.
22. Lau, J.C., Wagner-Rundell, N., Rodgers, C.T., Green, N.J., and Hore, P.J. (2010). Effects of disorder and motion in a radical pair magnetoreceptor. J. R. Soc. Interface *7* (*Suppl 2*), S257–S264.
23. Solov'yov, I.A., Mouritsen, H., and Schulten, K. (2010). Acuity of a cryptochrome and vision-based magnetoreception system in birds. Biophys. J. *99*, 40–49.
24. Möller, A., Sagasser, S., Wiltschko, W., and Schierwater, B. (2004). Retinal cryptochrome in a migratory passerine bird: A possible transducer for the avian magnetic compass. Naturwissenschaften *91*, 585–588.
25. Mouritsen, H., Janssen-Bienhold, U., Liedvogel, M., Feenders, G., Stalleicken, J., Dirks, P., and Weiler, R. (2004). Cryptochromes and neuronal-activity markers colocalize in the retina of migratory birds during magnetic orientation. Proc. Natl. Acad. Sci. USA *101*, 14294–14299.
26. Niessner, C., Denzau, S., Gross, J.C., Peichl, L., Bischof, H.J., Fleissner, G., Wiltschko, W., and Wiltschko, R. (2011). Avian ultraviolet/violet cones identified as probable magnetoreceptors. PLoS ONE *6*, e20091.
27. Watari, R., Yamaguchi, C., Zemba, W., Kubo, Y., Okano, K., and Okano, T. (2012). Light-dependent structural change of chicken retinal Cryptochrome4. J. Biol. Chem. *287*, 42634–42641.
28. Fusani, L., Bertolucci, C., Frigato, E., and Foà, A. (2014). Cryptochrome expression in the eye of migratory birds depends on their migratory status. J. Exp. Biol. *217*, 918–923.
29. Bolte, P., Bleibaum, F., Einwich, A., Günther, A., Liedvogel, M., Heyers, D., Depping, A., Wöhlbrand, L., Rabus, R., Janssen-Bienhold, U., and Mouritsen, H. (2016). Localisation of the putative magnetoreceptive protein cryptochrome 1b in the retinae of migratory birds and homing pigeons. PLoS ONE *11*, e0147819.
30. Niessner, C., Gross, J.C., Denzau, S., Peichl, L., Fleissner, G., Wiltschko, W., and Wiltschko, R. (2016). Seasonally changing cryptochrome 1b expression in the retinal ganglion cells of a migrating passerine bird. PLoS ONE *11*, e0150377.
31. Qin, S., Yin, H., Yang, C., Dou, Y., Liu, Z., Zhang, P., Yu, H., Huang, Y., Feng, J., Hao, J., et al. (2016). A magnetic protein biocompass. Nat. Mater. *15*, 217–226.
32. Kobayashi, Y., Ishikawa, T., Hirayama, J., Daiyasu, H., Kanai, S., Toh, H., Fukuda, I., Tsujimura, T., Terada, N., Kamei, Y., et al. (2000). Molecular analysis of zebrafish photolyase/cryptochrome family: Two types of cryptochromes present in zebrafish. Genes Cells *5*, 725–738.

33. Takeuchi, T., Kubo, Y., Okano, K., and Okano, T. (2014). Identification and characterization of cryptochrome4 in the ovary of western clawed frog Xenopus tropicalis. Zool. Sci. *31*, 152–159.

34. Phillips, J.B. (1996). Magnetic navigation. J. Theor. Biol. *180*, 309–319.

35. Putman, N.F., Endres, C.S., Lohmann, C.M., and Lohmann, K.J. (2011). Longitude perception and bicoordinate magnetic maps in sea turtles. Curr. Biol. *21*, 463–466.

36. Putman, N.F., Lohmann, K.J., Putman, E.M., Quinn, T.P., Klimley, A.P., and Noakes, D.L. (2013). Evidence for geomagnetic imprinting as a homing mechanism in Pacific salmon. Curr. Biol. *23*, 312–316.

37. Bottesch, M., Gerlach, G., Halbach, M., Bally, A., Kingsford, M.J., and Mouritsen, H. (2016). A magnetic compass that might help coral reef fish larvae return to their natal reef. Curr. Biol. *26*, R1266–R1267.

38. Kubo, Y., Akiyama, M., Fukada, Y., and Okano, T. (2006). Molecular cloning, mRNA expression, and immunocytochemical localization of a putative blue-light photoreceptor CRY4 in the chicken pineal gland. J. Neurochem. *97*, 1155–1165.

39. Mitsui, H., Maeda, T., Yamaguchi, C., Tsuji, Y., Watari, R., Kubo, Y., Okano, K., and Okano, T. (2015). Overexpression in yeast, photocycle, and in vitro structural change of an avian putative magnetoreceptor cryptochrome4. Biochemistry *54*, 1908–1917.

40. Oishi, T., Kawata, A., Hayashi, T., Fukada, Y., Shichida, Y., and Yoshizawa, T. (1990). Immunohistochemical localization of iodopsin in the retina of the chicken and Japanese quail. Cell Tissue Res. *261*, 397–401.

41. Kram, Y.A., Mantey, S., and Corbo, J.C. (2010). Avian cone photoreceptors tile the retina as five independent, self-organizing mosaics. PLoS ONE *5*, e8992.

42. Fischer, A.J., Stanke, J.J., Aloisio, G., Hoy, H., and Stell, W.K. (2007). Heterogeneity of horizontal cells in the chicken retina. J. Comp. Neurol. *500*, 1154–1171.

43. Uhlen, M., Bandrowski, A., Carr, S., Edwards, A., Ellenberg, J., Lundberg, E., Rimm, D.L., Rodriguez, H., Hiltke, T., Snyder, M., and Yamamoto, T. (2016). A proposal for validation of antibodies. Nat. Methods *13*, 823–827.

44. Kutta, R.J., Archipowa, N., Johannissen, L.O., Jones, A.R., and Scrutton, N.S. (2017). Vertebrate cryptochromes are vestigial flavoproteins. Sci. Rep. *7*, 44906.

45. Solov'yov, I.A., Domratcheva, T., Moughal Shahi, A.R., and Schulten, K. (2012). Decrypting cryptochrome: Revealing the molecular identity of the photoactivation reaction. J. Am. Chem. Soc. *134*, 18046–18052.

46. Cailliez, F., Müller, P., Gallois, M., and de la Lande, A. (2014). ATP binding and aspartate protonation enhance photoinduced electron transfer in plant cryptochrome. J. Am. Chem. Soc. *136*, 12974–12986.

47. Müller, P., Yamamoto, J., Martin, R., Iwai, S., and Brettel, K. (2015). Discovery and functional analysis of a 4th electron-transferring tryptophan conserved exclusively in animal cryptochromes and (6-4) photolyases. Chem. Commun. (Camb.) *51*, 15502–15505.

48. Helfer, G., Fidler, A.E., Vallone, D., Foulkes, N.S., and Brandstaetter, R. (2006). Molecular analysis of clock gene expression in the avian brain. Chronobiol. Int. *23*, 113–127.

49. Yamamoto, K., Okano, T., and Fukada, Y. (2001). Chicken pineal Cry genes: Light-dependent up-regulation of cCry1 and cCry2 transcripts. Neurosci. Lett. *313*, 13–16.

50. Haque, R., Chaurasia, S.S., Wessel, J.H., 3rd, and Iuvone, P.M. (2002). Dual regulation of cryptochrome 1 mRNA expression in chicken retina by light and circadian oscillators. Neuroreport *13*, 2247–2251.

51. Fu, Z., Inaba, M., Noguchi, T., and Kato, H. (2002). Molecular cloning and circadian regulation of cryptochrome genes in Japanese quail (*Coturnix coturnix japonica*). J. Biol. Rhythms *17*, 14–27.

52. Singh, D., Rani, S., and Kumar, V. (2013). Daily expression of six clock genes in central and peripheral tissues of a night-migratory songbird: evidence for tissue-specific circadian timing. Chronobiol. Int. *30*, 1208–1217.

53. Bailey, M.J., Chong, N.W., Xiong, J., and Cassone, V.M. (2002). Chickens' Cry2: Molecular analysis of an avian cryptochrome in retinal and pineal photoreceptors. FEBS Lett. *513*, 169–174.

54. Holmseth, S., Zhou, Y., Follin-Arbelet, V.V., Lehre, K.P., Bergles, D.E., and Danbolt, N.C. (2012). Specificity controls for immunocytochemistry: The antigen preadsorption test can lead to inaccurate assessment of antibody specificity. J. Histochem. Cytochem. *60*, 174–187.

55. Winklhofer, M., and Mouritsen, H. (2016). A room-temperature ferrimagnet made of metallo-proteins? bioRxiv. https://doi.org/10.1101/094607.

56. Hart, N.S. (2001). The visual ecology of avian photoreceptors. Prog. Retin. Eye Res. *20*, 675–703.

57. Marshak, D.W., and Mills, S.L. (2014). Short-wavelength cone-opponent retinal ganglion cells in mammals. Vis. Neurosci. *31*, 165–175.

58. Gunkel, M., Schöneberg, J., Alkhaldi, W., Irsen, S., Noe, F., Kaupp, U.B., and Al-Amoudi, A. (2015). Higher-order architecture of rhodopsin in intact photoreceptors and its implication for phototransduction kinetics. Structure *23*, 628–638.

59. Worster, S., Mouritsen, H., and Hore, P.J. (2017). A light-dependent magnetoreception mechanism insensitive to light intensity and polarization. J. R. Soc. Interface. Published online September 14, 2017. https://doi.org/10.1098/rsif.2017.0405.

60. Solov'yov, I.A., Chandler, D.E., and Schulten, K. (2007). Magnetic field effects in *Arabidopsis thaliana* cryptochrome-1. Biophys. J. *92*, 2711–2726.

61. Harris, S.R., Henbest, K.B., Maeda, K., Pannell, J.R., Timmel, C.R., Hore, P.J., and Okamoto, H. (2009). Effect of magnetic fields on cryptochrome-dependent responses in *Arabidopsis thaliana*. J. R. Soc. Interface *6*, 1193–1205.

62. Rozen, S., and Skaletsky, H. (2000). Primer3 on the WWW for general users and for biologist programmers. Methods Mol. Biol. *132*, 365–386.

63. Refinetti, R., Lissen, G.C., and Halberg, F. (2007). Procedures for numerical analysis of circadian rhythms. Biol. Rhythm Res. *38*, 275–325.

64. Kamphuis, W., Cailotto, C., Dijk, F., Bergen, A., and Buijs, R.M. (2005). Circadian expression of clock genes and clock-controlled genes in the rat retina. Biochem. Biophys. Res. Commun. *330*, 18–26.

65. Wei, R., Stewart, E.A., and Amoaku, W.M. (2013). Suitability of endogenous reference genes for gene expression studies with human intraocular endothelial cells. BMC Res. Notes *6*, 46.

66. Köhler, G., and Milstein, C. (1975). Continuous cultures of fused cells secreting antibody of predefined specificity. Nature *256*, 495–497.

67. Arnold, K., Bordoli, L., Kopp, J., and Schwede, T. (2006). The SWISS-MODEL workspace: A web-based environment for protein structure homology modelling. Bioinformatics *22*, 195–201.

68. Biasini, M., Bienert, S., Waterhouse, A., Arnold, K., Studer, G., Schmidt, T., Kiefer, F., Gallo Cassarino, T., Bertoni, M., Bordoli, L., and Schwede, T. (2014). SWISS-MODEL: Modelling protein tertiary and quaternary structure using evolutionary information. Nucleic Acids Res. *42*, W252–W258.

69. Bordoli, L., Kiefer, F., Arnold, K., Benkert, P., Battey, J., and Schwede, T. (2009). Protein structure homology modeling using SWISS-MODEL workspace. Nat. Protoc. *4*, 1–13.

70. Schmalen, I., Reischl, S., Wallach, T., Klemz, R., Grudziecki, A., Prabu, J.R., Benda, C., Kramer, A., and Wolf, E. (2014). Interaction of circadian clock proteins CRY1 and PER2 is modulated by zinc binding and disulfide bond formation. Cell *157*, 1203–1215.

71. Brautigam, C.A., Smith, B.S., Ma, Z., Palnitkar, M., Tomchick, D.R., Machius, M., and Deisenhofer, J. (2004). Structure of the photolyase-like domain of cryptochrome 1 from *Arabidopsis thaliana*. Proc. Natl. Acad. Sci. USA *101*, 12142–12147.

72. Phillips, J.C., Braun, R., Wang, W., Gumbart, J., Tajkhorshid, E., Villa, E., Chipot, C., Skeel, R.D., Kalé, L., and Schulten, K. (2005). Scalable molecular dynamics with NAMD. J. Comput. Chem. *26*, 1781–1802.

73. MacKerell, A.D., Bashford, D., Bellott, M., Dunbrack, R.L., Evanseck, J.D., Field, M.J., Fischer, S., Gao, J., Guo, H., Ha, S., et al. (1998). All-atom

empirical potential for molecular modeling and dynamics studies of proteins. J. Phys. Chem. B *102*, 3586–3616.

74. Mackerell, A.D., Jr., Feig, M., and Brooks, C.L., 3rd. (2004). Extending the treatment of backbone energetics in protein force fields: Limitations of gas-phase quantum mechanics in reproducing protein conformational distributions in molecular dynamics simulations. J. Comput. Chem. *25*, 1400–1415.
75. Best, R.B., Zhu, X., Shim, J., Lopes, P.E., Mittal, J., Feig, M., and Mackerell, A.D., Jr. (2012). Optimization of the additive CHARMM all-atom protein force field targeting improved sampling of the backbone φ, ψ and side-chain χ(1) and χ(2) dihedral angles. J. Chem. Theory Comput. *8*, 3257–3273.
76. Sjulstok, E., Olsen, J.M., and Solov'yov, I.A. (2015). Quantifying electron transfer reactions in biological systems: What interactions play the major role? Sci. Rep. *5*, 18446.
77. Lüdemann, G., Solov'yov, I.A., Kubař, T., and Elstner, M. (2015). Solvent driving force ensures fast formation of a persistent and well-separated radical pair in plant cryptochrome. J. Am. Chem. Soc. *137*, 1147–1156.
78. Solov'yov, I.A., Domratcheva, T., and Schulten, K. (2014). Separation of photo-induced radical pair in cryptochrome to a functionally critical distance. Sci. Rep. *4*, 3845.
79. Feller, S.E., Zhang, Y., Pastor, R.W., and Brooks, B.R. (1995). Constant pressure molecular dynamics simulation: The Langevin piston method. J. Chem. Phys. *103*, 4613–4621.

STAR★METHODS

KEY RESOURCES TABLE

REAGENT or RESOURCE	SOURCE	IDENTIFIER
Antibodies		
See Table S5 for primary antibodies	N/A	N/A
See Table S6 for secondary antibodies	N/A	N/A
Anti-rat kappa light chain antibodies	ATCC	Cat#TIB172; RRID: CVCL_G154
Mouse anti rat IgG1 (ATCC name: RG11/39.4)	ATCC	Cat#TIB170; RRID: CVCL_G151
Mouse anti rat IgG2a (ATCC name: RG7/1.30)	ATCC	Cat#TIB173; RRID: CVCL_G152
Mouse anti rat IgG2b (ATCC name: RG7/11.1)	ATCC	Cat#TIB174; RRID: CVCL_G153
Chemicals, Peptides, and Recombinant Proteins		
TRIzol Reagent	Life technologies	Cat#15596
DNase I	Invitrogen	Cat#18068015
Superscript III Reverse Transcriptase	Life technologies	Cat#18080-044
Go Taq Long PCR Master Mix	Promega	Cat#M4021
Xho I Fast Digest enzyme	Thermo Fisher Scientific	Cat#FD0694
Hind III Fast Digest enzyme	Thermo Fisher Scientific	Cat#FD0504
Lipofectamine2000 reagent	Invitrogen	Cat#11668027
erCry1a-GFP	[29]	N/A
erCry1b-GFP	[29]	N/A
erCry2-GFP	this work	N/A
erCry4-GFP	this work	N/A
Critical Commercial Assays		
QiaQuick PCR Purification Kit	QIAGEN	Cat#28106
Rapid DNA Dephos & Ligation Kit	Roche	Cat#04898117001
QuantiTect Reverse Transcription Kit	QIAGEN	Cat#205310
1-stepTM Ultra TMB-Elisa	Thermo Fisher Scientific	Cat#34028
FastStart Essential DNA Green Master	Roche	Cat#06402712001
Deposited Data		
erCry4 sequence	this work	GenBank: KX890129
Experimental Models: Organisms/Strains		
Lou/c rats	From rats of presumed Wistar origin kept at the Université Catholique de Louvain	N/A
Oligonucleotides		
See Tables S3 and S4 for lists of primers	N/A	N/A
Software and Algorithms		
Geneious R6 student personal	Biomatters Ltd.	https://www.geneious.com/
Primer 3	[62]	http://bioinfo.ut.ee/primer3-0.4.0/
SPSS package 23	IBM SPSS Inc.	N/A
Cosinor	[63]	http://www.circadian.org/softwar.html
Other		
pGEM-T Easy vector	Promega	Cat#A1360
pTurboGFP-N vector	Evrogen	Cat#FP512

CONTACT FOR REAGENT AND RESOURCE SHARING

Further information and requests for reagents may be directed to and will be fulfilled by the Lead Contact, Henrik Mouritsen (henrik.mouritsen@uni-oldenburg.de).

EXPERIMENTAL MODEL AND SUBJECT DETAILS

European robins (*Erithacus rubecula*) were wild-caught in the vicinity of the university campus using mist nets. All animal procedures were approved by the Animal Care and Use Committees of the Niedersächsisches Landesamt für Verbraucherschutz und Lebensmittelsicherheit (LAVES, Oldenburg, Germany). European robins 1 to 16 in Table S1 were housed singly in a non-magnetic outdoor aviary with access to fresh air and to the natural celestial cues. The remaining European robins were housed singly indoors under local photoperiodic conditions in custom-built iron-free cages measuring 100x50x40cm. We also collected the retinae of nine European robins, which were killed for other experiments, for Cry4 sequencing and twelve European robins for immunohistochemistry. The domestic chickens (*Gallus gallus*; five for immunohistochemistry and 20 for qRT-PCR, see Table S2) were hatched in the animal facility of the university and housed indoors under local photoperiodic conditions.

METHOD DETAILS

Amplification and identification of the cDNA sequences

For sequence identification and qPCR, the retinae were collected from birds killed by decapitation. Eyes were removed immediately and the retina, free of vitreous, was put into ice-cold TRIzol Reagent (Life Technologies, Carlsbad, CA, USA), shock-frozen in liquid nitrogen and stored at –80°C until RNA extraction. The total RNA of one retina from each bird was isolated using the TRIzol Reagent (Life Technologies) according to manufacturer's instructions. After treatment with DNase I (Invitrogen, Carlsbad, CA, USA), the RNA was copied into first-strand cDNA using Superscript III Reverse Transcriptase (Life Technologies) following the manufacturer's protocol. Total nucleotide sequence of European robin *Cry4* as well as of the chicken opsin genes and the reference genes for qRT-PCR (glutamate receptor 2 [*GluR2*], TATA-box binding protein [*Tbp*], and protein kinase C alpha [*Prkca*]) were amplified from retinal cDNA templates. The primers had been designed to anneal to evolutionary conserved regions identified after alignment of reported avian homologs. Details of primer sequences and reaction conditions are summarized in Table S3. PCR amplification of the cDNA sequences was performed with the GoTaq® Long PCR Master Mix (Promega, Madison, WI, USA). The cycle conditions were: 1 cycle denaturation at 95°C (5 min), 35 cycles at 94°C (15 s), X °C (gene-specific temperature see Table S3, 30 s; *erCry4* and the chicken opsins: 1 min), 72°C (1 min/kb), with a final extension of 10 min at 72°C. After purification using the QIAquick PCR Purification Kit (QIAGEN, Hilden, Germany), PCR products of the appropriate length were either sent for sequencing directly (*erTbp*, *erGluR2*), or cloned into the pGEM®-T Easy vector (Promega) for subsequent sequencing by an external contractor (LGC Genomics, Berlin, Germany). The amplified sequences of erCry4 and of the chicken opsins were digested with XhoI/HindIII restriction enzymes (Thermo Fisher Scientific, Waltham, MA, USA) and cloned into the expression vector pTurboGFP-N (Evrogen, Moscow, Russia) according to the protocol for the Rapid DNA Dephos & Ligation Kit (Roche Diagnostics, Rotkreuz, Switzerland). DNA identity of *erCry4* and similarities between the individuals were analyzed with Geneious R6 student personal (Biomatters Ltd, Auckland, New Zealand).

Quantitative reverse transcriptase polymerase chain reaction

Total RNA from birds listed in Table S1 and S2 was isolated from one retina of each bird using TRIzol Reagent (Invitrogen). RNA concentration was determined using the Infinite® 200 PRO instrument (Tecan, Männedorf, Switzerland). For each sample, 1 μg total RNA was reversely transcribed using the QuantiTect® Reverse Transcription Kit (QIAGEN) according to the manufacturer's instructions. As negative control, samples of each batch of reverse transcription were pooled and incubated with primer mix lacking reverse transcriptase. The obtained cDNA was diluted 1/20 in 0.1x TE buffer and stored at –20°C until use. Primers were designed using Primer3 [62] to amplify products of predicted sizes in the range of 50 to 147 bp from cDNA templates. The primer positions were selected to flank predicted introns in order to facilitate detection of any genomic DNA contamination in the cDNA preparations. Primer sequences are listed in Table S4. The efficiency of the primer pairs for all genes investigated was determined by performing standard curves. For each primer pair, dissociation curves were generated to assess specificity. Only single products and no primer dimers were detected. 1/400 of the total cDNA yield (2.5 ng cDNA) was used for each qRT-PCR reaction. Each qRT-PCR reaction contained 1 μl of a 2 μM primer solution, 5 μL FastStart Essential DNA Green Master (Roche) and 1 μl cDNA in a 10 μL reaction volume. All samples were run in triplicate. The reaction was run at default settings (pre-incubation 95°C, 600 s; 3 step amplification 95°C, 10 s; 55°C, 10 s; 72°C, 10 s; 45 cycles) on the LightCycler® 96 Instrument (Roche). For between-sample normalization, genes were selected based on reference gene data from literature [48, 64, 65].

Antibody generation

We produced two different antibodies against Cry4, one polyclonal (Cry4) and one monoclonal (erCry4 3C2) antibody. Since the Cry4 sequence of European robin was not known at the beginning of this project, the polyclonal primary antibody (custom-made by Aldevron, Freiburg, Germany; see Table S5) was directed against the C-terminal part of the Cry4 protein from Zebra finch, *Taeniopygia guttata* (amino acid 489-512, GenBank accession number XM_012570954.1), which was the only known songbird Cry4 sequence at that time. While working on the current project, we identified the cDNA and amino acid sequence of Cry4 from European robin. Two of the 23 amino acids were different when the European robin and zebra finch sequences were compared (antibody amino acids 4 and 21). Therefore, we also produced a monoclonal antibody (erCry4 3C2) directed against the 23 amino acids in the European robin (Table S5).

For the generation of the monoclonal antibodies, peptides comprising amino acids HRTAQLTRDDADDPMEIKVKRDH from erCry4, amino acids MHPPRPTTDLPEDF from blue opsin, and amino acids ARRRHEEEDTTRD from iodopsin were synthesized and coupled to ovalbumin (Ova) and biotin for immunisation and testing, respectively (Peps4LS, Heidelberg, Germany). Lou/c rats were immunized subcutaneously (s.c.) and intraperitoneally (i.p.) with a mixture of 50 μg Ova-coupled peptide in 500 μl PBS, 5 nmol CpG2006 (TIB MOLBIOL, Berlin, Germany), and 500 μl incomplete Freund's adjuvant. After six weeks, a boost without Freund's adjuvant was given i.p. and s.c. three days before fusion. Fusion of the myeloma cell line P3X63-Ag8.653 with the rat immune spleen cells was performed using polyethylene glycol 1500 according to standard procedure [66]. After fusion, the cells were plated in 96-well plates using RPMI 1640 with 20% fetal calf serum (FCS), penicillin/streptomycin, glutamine, pyruvate, non-essential amino acids, and HAT medium supplement (Sigma-Aldrich, Munich, Germany). Hybridoma supernatants were tested in an enzyme-linked immunoassay using biotinylated peptides (0.2 μg/ml) bound to avidin-coated plates. After blocking with PBS/2% FCS, hybridoma supernatants were added for 30 min. After one wash with PBS, bound antibodies were detected with a cocktail of horseradish peroxidase (HRP)-conjugated mouse antibodies against the four rat IgG isotypes (TIB173 IgG2a, TIB174 IgG2b, and TIB170 IgG1 from ATCC, Manassas, VA, USA; IgG2c homemade). HRP was visualized with ready to use TMB substrate (1-StepTM Ultra TMB-ELISA, Thermo Fisher Scientific). The hybridoma cells of one erCry4-, one blue opsin- and one iodopsin-reactive supernatant were cloned at least twice by limiting dilution. The IgG subclass was determined in an ELISA assay with mouse anti-rat kappa light chain antibodies (TIB172, ATCC) as capture and HRP-coupled mouse anti-rat IgG subclass-specific antibodies for detection. Cell culture supernatants of Cry4 3C2 (rat IgG2a/k), blue opsin 2D6 (rat IgG1/k) and iodopsin 3B1 (rat IgG2c/k) were used in this study.

Immunohistochemistry

Eyecups from twelve European robins and five chickens were prepared by cornea dissection followed by removal of the lens and vitreous body. After fixation in 4% PFA/PBS for 20 min and washing in PBS, the tissues were cryoprotected overnight at 4°C in 30% saccharose solution in 0.1 M PBS and embedded in cryoblock at −20°C. Vertical retinal sections of 20 μm were cut on a cryostat, collected on gelatinised Menzel SuperFrost Plus slides (Thermo Fisher Scientific) and heat-fixed at 37°C for 3 hr. As buffer, TBS with 0.3% Triton X-100 was used. After washing, the slices were bleached by immersion of the retinal slices for 30 min in 5 mL 1.8% NaCl, 4 mL 30% H_2O_2, 1 mL H2O and one drop of ammonia solution to make the outer segments visible for microscopy. After extensive washing, the cryosections were blocked in buffer with 10% FCS for 60 min at room temperature. The primary antibody (Table S5) incubation (with 2% FCS) was performed overnight at 4°C. Both Cry4 antibodies were visualized with the respective Alexa 488-conjugated secondary antibodies, whereas the antibodies against the opsins and calbindin were visualized with the respective Alexa 555-conjugated secondary antibodies (Table S6). All enhancing antibodies and secondary antibodies were incubated for 2 hr at room temperature. All slides were covered with Vecta shield (Vector Laboratories Inc., Burlingame, CA, USA) and a coverslip. To test the specificity of the Cry4 antibodies, in one set of controls, the primary antibody was pre-adsorbed with the peptide in a ratio of 1:10 for 4 hr and, in a second set of controls, the polyclonal Cry4 antibody was replaced by the pre-immune serum. All other procedures were identical to those described above.

Cell culture and protein expression

COS-1 and HEK cells were maintained in DMEM with 10% Fetal Calf Serum and 1% antibiotics/antimyotics (Life Technologies). For protein expression, erCry1a, erCry1b, erCry2, erCry4, rhodopsin, UVopsin, BlueOpsin, GreenOpsin and iodopsin were expressed as fusion proteins with GFP from the respective generated pTurbo-GFP-N vectors using 2 μl Lipofectamine 2000 reagent (Invitrogen) per μg DNA in OptiMEM medium (Life technologies) following the manufacturer's protocol. The cells were harvested 48 hr after transfection.

Immunocytochemistry of transfected cells

48 hr after transfection, the cells were washed in phosphate buffered saline (PBS) twice for 5 min each followed by a 15 min fixation with 3% paraformaldehyde. Then, the cells were washed in PBS twice for 5 min each and incubated for 30 min with PBS including 0.1% Triton X-100 to enhance the permeability of the cell membrane. Afterward, the cells were blocked with 10% donkey or goat serum depending on the origin of the secondary antibody. To ensure that both Cry4 antibodies only detected the Cry4 protein, separate wells were transfected with a pTurboGFP-N vector coding for erCry1a-GFP, erCry1b-GFP, erCry2-GFP or erCry4-GFP fusion proteins. The incubation with the primary antibody took place at 4°C over night. After washing and enhancement of the monoclonal erCry4 antibody (for 2 hr at room temperature, see Table S5), the cells were incubated for 2 hr at room temperature with the respective Alexa 555-conjugated secondary antibody (see Table S6). Monoclonal antibodies against blue opsin and iodopsin were tested on HEK293 cells expressing ggRhodopsin-GFP, ggUVopsin-GFP, ggBlueOpsin-GFP, ggIodopsin-GFP and ggGreenOpsin-GFP. The transfection and staining procedures were performed as for the Cry4 antibodies. The coverslips were rinsed in PBS before being mounted with Vecta shield (Vector Laboratories).

Western blot analysis

48 hr after transfection, the cells were washed three times 5 min each in phosphate buffered saline (PBS), harvested, and centrifuged (3,000 rpm for 5 min at 4°C). The cell pellet was resuspended in lysis buffer containing 1% Nonidet P-40 Lysis Buffer (Amresco, Solon, OH, USA), 0.15 M NaCl, 0.05 M Tris HCl and one cOmplete ULTRA tablet (Roche), incubated for 30 min at room temperature and vortexed every 10 min. The insoluble membrane fraction was separated by centrifugation for 15 min at 14,000 rpm and 4°C. The

soluble, Cry4-GFP protein containing part was used for further analysis. The total protein concentration was measured by Bradford protein assay according to the manufacturer's protocol (BioRad, Hercules, CA, USA). SDS-PAGE (8% gels). Western blot analysis was performed with 50 μg of protein mixed with Roti-Load 1 loading dye (Carl Roth, Karlsruhe, Germany). Protein transfer from gel to membrane took place in a Fastblot B33 system using a 200 V and 200 mA separation current for 25 min followed by 25 min with a 200 V and 299 mA separation current. For polyclonal antibody detection, the nitrocellulose membrane (Whatman, Sigma Aldrich) was incubated for 1 hr in Roti Block solution (Roth) and for the monoclonal antibodies, 1% milk powder (Roth) in buffer was used. The membranes were incubated with primary antibodies (Table S5) diluted in TBS-Tween (20 mM Tris/HCl, 150 mM NaCl, 0.3% Tween, pH 7.4) overnight at 4°C. The monoclonal antibodies against blue opsin and iodopsin were used in a dilution of 1:20. After washing, the monoclonal antibodies were additionally enhanced with the respective anti-subclass-specific antibody (Table S5) for 2 hr at room temperature under permanent shaking. After incubation with HRP-conjugated secondary antibodies (Table S6), a chemiluminescence procedure was performed with Super Signal West Pico chemiluminescent substrates (Thermo Fisher Scientific), and Fuji medical X-ray film (Fujifilm, Tokyo, Japan) in a dark room. To test the specificity of the polyclonal Cry4 antibody, the antibody was pre-incubated with the immunisation peptide in a ratio of 1:10 for 4 hr under permanent shaking. In another experiment, the polyclonal Cry4 antibody was replaced by the pre-immune serum. For the control stainings, the same secondary antibodies with identical conditions and procedures were used.

Confocal microscopy

Confocal micrographs of fluorescent retinae and transfected cells were analyzed with a TCS SP2 or SP8 confocal microscope (Leica Camera AG, Wetzlar, Germany) using the 488 and 555 nm lines. Scanning was performed with the oil immersion 40x HPX PL APO (NA 1.25 or 1.3) objective at a resolution of either 1024x1024 or 2048x2048 pixels. Images were processed in brightness and contrast superimposed using either ImageJ (NIH, Bethesda, MD, USA) or Adobe Illustrator CS5 (Adobe, San Jose, CA, USA). All images of the same experiment were taken with the same microscope settings.

Computational modeling

A three dimensional structure of erCry4 was built based on the amino acid sequence determined experimentally in this paper, using the Swiss-model workspace [67–69]. Mouse cryptochrome 1a (PDB ID: 4CT0) was used as a template for the homology model, which covered 91% of the amino acid sequence with an amino acid sequence identity of 52% [70] to erCry4 (Figure S2A). The crystal structure of mouse cryptochrome does not include a bound FAD cofactor. Therefore, for the homology model of erCry4, the FAD moiety was placed inside the erCry4 protein as in the structure of *Arabidopsis thaliana* cryptochrome 1 (atCry1, PDB ID: 1U3C) [71] by superimposing the structure of the protein backbone with the backbone of the constructed homology model of erCry4. The obtained homology model was then dynamically equilibrated for 225 ns, using the NAMD molecular dynamics (MD) package [72], and the stability of the equilibrated structure was checked by further simulation over 275 ns. All simulations were carried out using the CHARMM36 force field [73–75] for proteins, along with an earlier parameterisation for FAD successfully employed in several MD studies of cryptochrome [76–78]. A time step of 2 fs was used and the temperature was controlled at 310 K using the Langevin thermostat. Similarly, the pressure was held at 1 atm with the Langevin Barostat [79]. The ShakeH algorithm was used to keep bonds involving hydrogen atoms at fixed lengths. Periodic boundary conditions were adopted in all MD simulations and the Particle Mesh Ewald summation method was employed for evaluating Coulomb forces. The van der Waals energy was calculated using a smooth cut-off of 12 Å with a switching distance of 10 Å.

QUANTIFICATION AND STATISTICAL ANALYSIS

All results are presented as means ± SEM. For the circadian expression data, the p value of a one-way analysis of variance (ANOVA) was calculated based on the normalized data (SPSS package 23, SPSS Inc., IL, USA) to test for a statistically significant difference among the different groups. If the ANOVA indicated such differences, a post hoc t test was performed (Tukey HSD). To evaluate rhythmicity in gene expression, the cosine curve fitting (Cosinor) method was performed with software available at http://www.circadian.org/softwar.html [63]. Significance of Cosinor analysis was defined by the noise/signal of amplitude calculated from the ratio *SE(A)/A.* Expression was considered to display a daily rhythm if it had both $p < 0.05$ by ANOVA and $SE(A)/A < 0.3$ by Cosinor analysis. To analyze the season-dependent expression data, a Mann-Whitney test was performed using SPSS.

DATA AND SOFTWARE AVAILABILITY

The accession number for the erCry4 sequence reported in this paper is GenBank: KX890129.